Machine learning guided development of high-performance nano-structured nickel electrodes for alkaline water electrolysis

Jensen, Veronica Humlebæk; Moretti, Enzo Raffaele; Busk, Jonas; Christiansen, Emil Howaldt; Skov, Sofie Marie; Jacobsen, Emilie; Kraglund, Mikkel Rykær; Bhowmik, Arghya; Kiebach, Ragnar

Published in:
Applied Materials Today

Link to article, DOI:
10.1016/j.apmt.2023.102005

Publication date:
2023

Document Version
Publisher's PDF, also known as Version of record

Applied Materials Today 35 (2023) 102005

Contents lists available at ScienceDirect

Applied Materials Today

journal homepage: www.elsevier.com/locate/apmt

Machine learning guided development of high-performance nano-structured nickel electrodes for alkaline water electrolysis

Veronica Humlebæk Jensen, Enzo Raffaele Moretti *, Jonas Busk, Emil Howaldt Christiansen, Sofie Marie Skov, Emilie Jacobsen, Mikkel Rykær Kraglund, Arghya Bhowmik, Ragnar Kiebach *

Department of Energy Conversion and Storage, Technical University of Denmark, Campus, Anker Engelunds Vej, Lyngby 2800 Denmark

ARTICLE INFO

Keywords:
Water electrolysis
Nano catalyst
Hydrogen evolution reaction
Bayesian optimization
Technical electrodes
Human in the loop

ABSTRACT

Utilizing a human in the loop Bayesian optimisation paradigm based on Gaussian process regression, we optimized an Ni electrodeposition method to synthesize nano-structured, high-performance hydrogen evolution reaction electrodes. Via exploration-exploitation stages, the synthesis process variables current density, temperature, ligand concentration and deposition time were optimized influencing the deposition layer morphology and, consequently, hydrogen evolution reaction activity. The resulting structures range from micrometre-sized, star-shaped features to nano-sized sandpaper-like structures with very high specific surface areas and good hydrogen evolution reaction activity. Using the overpotential at 10 mA cm^{-2} as the figure of merit, hydrogen evolution reaction overpotentials as low as -117 mV were reached, approaching the best known technical high surface area electrodes (e.g. Raney Ni). This is achieved with considerably fewer experiments than what would have been necessary with a linear grid search, as the machine learning model could capture the unintuitive interdependencies of the synthesis variables.

1. Introduction

In order to reduce global carbon emission it is not enough to switch from fossil fuels to renewable energy sources. The green transition will rely heavily on the availability of green hydrogen as an energy carrier. Both for energy storage applications, to counteract the inherently intermittent nature of wind and solar power, but also as a chemical precursor for e-fuels and to decarbonize industry sectors such as cement and steel production [1,2].

To reach the global goal of carbon neutrality, the demand for green hydrogen will increase substantially. The International Energy Agency's Net Zero Emissions Scenario for 2050 assumes that a total installed electrolyser capacity of 850 GW by 2030 and 3600 GW by 2050 will be needed - a roughly 7000-fold increase in less than three decades from the 0.5 GW that were operational by the end of 2021 [3]. This implies that low cost materials, simple fabrication methods and TWh scalability are hard requirements for the industrial application of any new technology in this field. Irrespective of this, novel electrolysers also need to operate more efficiently than current systems in order to be economically feasible. Highly active catalyst materials comprised of abundant elements present a pathway to achieve these objectives.

Alkaline water electrolysis (AWE) is the most mature commercialized electrolysis technology available. Nevertheless, AWE systems still struggle with corrosion and low operating current densities [4–6]. For the hydrogen evolution reaction (HER), noble metals such as platinum show good catalytic performance but remain unsuitable at large and industrial scales due to their prohibitive cost and scarcity [5]. Nickel (Ni) on the other hand, is relatively inexpensive, earth abundant, has been studied widely as an alkaline electrolysis catalyst and is often used in commercial electrolysers due to its decent catalytic activity and stability in alkaline media [5,7]. Its performance as a HER catalyst can be further improved by secondary elements such as cobalt and molybdenum or by increasing the amount of catalytic active sites via high surface area secondary Ni structures [7]. Raney-type Ni is a well-known example of high surface area Ni catalysts with outstanding performance [8] yet is difficult to synthesise and suffers from deactivation under intermittent operation.

Electrodeposition is a facile, scalable, fast and in-expensive deposition method [5,9] proven to be capable of creating different secondary Ni structures [5,10–14]. The structure deposited through electrodeposition depends strongly on plating parameters such as current density, deposition time, solution temperature, concentration and pH, which

* Corresponding authors.
E-mail addresses: enzomo@dtu.dk (E.R. Moretti), woki@dtu.dk (R. Kiebach).

https://doi.org/10.1016/j.apmt.2023.102005
Received 31 August 2023; Received in revised form 13 November 2023; Accepted 20 November 2023
Available online 27 November 2023

creates a large parameter space. Developing well performing secondary Ni structures is a challenging and time consuming process, requiring numerous experiments guided by intuition, trials and errors. One way of speeding up such parameter optimization task is by applying machine learning (ML) techniques. ML models have been used to accelerate the computational communities discovery of energy materials, for example in batteries, solar cells and catalysts [15–18]. Being a data driven method, such an approach relies on the controlled generation of high fidelity large volume computational data. It is much more challenging with experimental data sources due to small data regime and noisy observations. Recently ML based "design of experiments" for materials optimization has increasingly attracted interest in experimental materials synthesis community from an accelerated discovery perspective as high throughput experiments become accessible [19,20].

Experimental search campaigns with AI guided design of experiments and a closed-loop feedback can outperform human intuition driven drastically as cognitive limitations of human researchers impede the optimal exploration of complex parameter spaces. Recent breakthroughs in AI driven experiment design have focused on organic reaction planning and optimization [21–23] but a handful of recent articles demonstrate the usefulness of AI guided optimization towards synthesis of solid state materials [24–27] as well.

In this work, we showcase the benefits of applying AI guided iterative optimization even outside of autonomous labs, where Ni based electrodes for the alkaline HER are optimized. Guided by an exploration-exploitation scheme we vary the process parameters of the Ni electrodeposition to optimize the electrochemically active surface area (ECSA), using the HER overpotential at a given current density as the figure of merit for the underlying Gaussian process regression model. The Bayesian optimization in an iterative approach helps us choose the most promising parameter sets for the next synthesis batch based on the expected value of overpotential and the related uncertainty. This allowed us to obtain large improvements in catalytic performance and HER activities approaching the Raney-Ni domain in a complex search space with reduced experimental effort.

2. Material and methods

2.1. Experimental

2.1.1. Materials

KOH (ACS reagent, ≥ 85 %), $NiCl_2 \bullet 6H_2O$ (≥ 98 %), H_3BO_3 (ACS Reagent ≥ 99.8 %), ethylenediamine dihydrochloride (EDA, 98 %) and HCl (37 wt%) were supplied by Sigma Aldrich, while NH_4OH (25 %) was supplied by Alfa Aesar. Perforated Ni plate with a 300 μm thickness, 1 mm hole size and 0.7 mm hole spacing was used as substrate. Ni plates (99.95 %) were supplied by Alfa Aesar.

2.1.2. Electrode preparation

As electrode substrate, perforated Ni plates were cut to samples with a size of 2.5 cm • 2.5 cm. To ensure a clean and smooth surface, the samples went through a three step pre-treatment process. To remove organic substances the substrate was ultrasonicated in an acetone-ethanol (1:1) solution for 30 min whereafter the substrate was submerged in 3 M HCl for 30 s to remove Ni oxides. Lastly, to ensure good adhesion, a Ni coating was deposited. Between each step the substrate was rinsed with deionized water.

To deposit the nanostructured Ni we adopted a process from Zhou et al. [28] using a solution composed of $NiCl_2 \bullet 6H_2O$, H_3BO_3 and ethylenediamine dihydrochloride (EDA) as shown in Table 1. The reactants were dissolved in deionized water by stirring the solution while heating the solution slowly to 65 °C. Once the temperature had stabilized the pH was adjusted to 4 by dropwise addition of 10 % NH_4OH. To ensure even deposition on both sides of the substrate, two 10 cm • 2 cm • 0.16 cm Ni plate pieces were used as anodes. The exposed area of the anodes was limited to 2 cm • 2 cm with polyester tape (1280, 3 M), while the distance to the Ni substrate was 3 cm (see step 1 in Fig. 1). A wide neck bottle with a total solution volume of ca. 550 ml was used as the synthesis reactor. The reactor was placed in a heated water bath on a hot plate for improved temperature stability. Current was supplied by an Elektro-Automatik EA-PS 5040–40A power supply, by connecting the electrodes with crocodile clamps. The deposition was started ca. 1 hour after the temperature had reached the target temperature by applying a constant current for a specified time. Detailed operating conditions are shown in Table 1.

Table 1
The composition and operating condition intervals of the solution used for electrodepositing nano-structured Ni.

Bath composition	Concentration
$NiCl_2 \bullet 6H_2O$	200 g L^{-1}
H_3BO_3	25 g L^{-1}
EDA	200 g L^{-1}
10 % NH_4OH	–
Operating conditions	**Value**
Current density	4–160 mA cm^{-2}
Temperature	20–65 °C
Time	2–64 min
pH	4.0
Anodes	2 cm • 2 cm • 0.16 cm Ni
Stirring	60 rpm

The electrodeposition solution was reused for multiple samples. To ensure reproducibility the solution stability was monitored by synthesising control samples on a regular basis. For more information on the solution stability see Fig. S1 in the supplementary information (SI).

2.1.3. Electrochemical characterization

The electrochemical measurements were conducted using a conventional three electrode setup connected to a Gamry Reference 600 Potentiostat. 1 M KOH was used as an electrolyte, a 2.5 cm · 2.5 cm perforated Ni plate as counter electrode and a reversible hydrogen electrode (RHE, Gaskatel mini-HydroFlex) as a reference electrode.

Before testing, the electrodes were preconditioned by potential sweeps from 200 to −400 mV vs. RHE (5x) using a scan rate of 20 mV s^{-1}.

Subsequently, 5 cyclic voltammetry (CV) scans were recorded in a region from +85 to −40 mV vs. RHE at different scan rates (10, 20, 50, 75 and 100 mV s^{-1}) to estimate the double layer capacitance. For each scan rate the respective charging current (i_c) is determined in a linear region according to Equation 1:

$$i_c = \sum_{n=1}^{N} \frac{1}{N} \left(\frac{\left| i_n^{forward} - i_n^{backward} \right|}{2} \right)$$

Where n are given datapoints across the linear region and N the total amount of datapoints. Plotting the scan rate vs. charging current yields a straight line with a slope equal to the specific double layer capacitance (C_{dl}), which is directly proportional to the electrochemical surface area (ECSA) and by association the roughness factor (R_f), as shown in Equation 2.

$$ECSA = A_{geo} \frac{C_{dl}}{C_s} = A_{geo} R_f$$

Where A_{geo} is the geometrical area of the electrode and C_s the specific capacitance, which according to P. Connor et al [29] can be estimated to 20 μF cm^{-2} for metallic surfaces.

The solution resistance was estimated using electrochemical impedance spectroscopy (EIS) performed at open circuit potential from 10^5 to 1 Hz using an AC amplitude of 10 mV, and later used for IR compensation (95 %).

To evaluate the electrode performance linear sweep voltammetry (LSV) was conducted using a scan rate of 1 mV s^{-1} in the range 200−400 mV vs. RHE. From the compensated LSV curves the

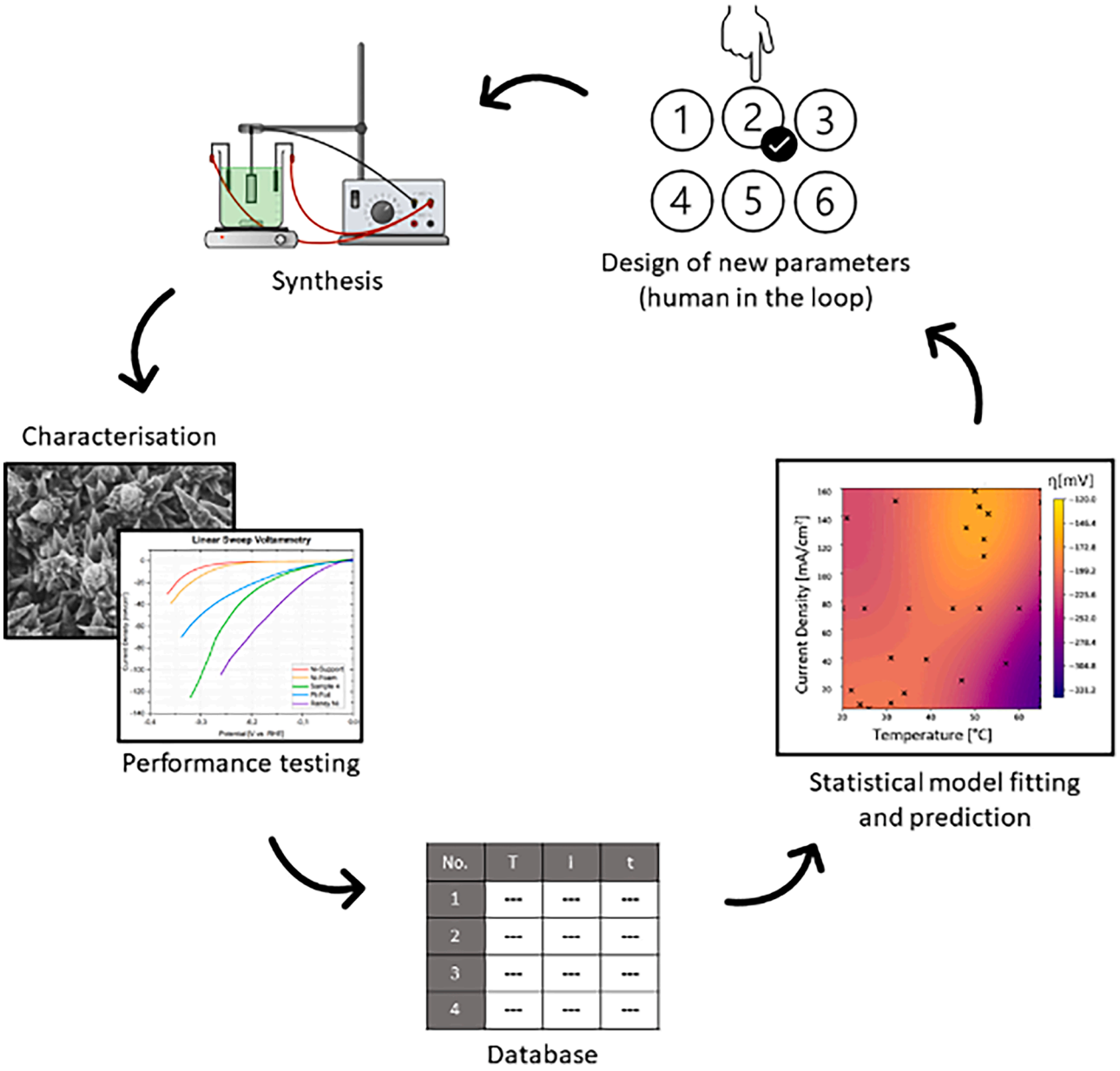

Fig. 1. The optimization process can be described by an iterative loop of five steps. (1) Electrodes are synthesized in batches of 5–6 according to Section 2.1.2. (2) Electrodes are tested and characterized using the method described in Sections 2.1.3 and 2.1.4. (3) The used synthesis parameters and performance metric (η at 10 mA cm^{-2}) are fed into a database. (4) Bayesian optimization, including a sensitivity analysis, is conducted using the database, resulting in a heat map of mean predicted overpotentials for any given combination of synthesis parameters. (5) Synthesis parameters for next batch are chosen manually based on the heat map (human in the loop). The drawing of the setup has been created with Chemix (https://chemix.org).

overpotential at 10 mA cm^{-2} (η_{10}) was extracted.

2.1.4. Physical characterization

Images of the electrodeposited microstructure were acquired using a high resolution scanning electron microscope (SEM, Zeiss Merlin). X-ray photoelectron spectroscopy (XPS) was recorded with a Thermo Fischer Scientific ESCALAB 250Xi.

2.2. Machine learning methods

To guide the experiment towards optimal input parameters, we applied a human-in-the-loop Bayesian optimization (BO) approach. Various machine learning techniques can be utilized for such optimization problems, although some require very large data sets, such as neural networks. In this study, relatively few data points are being generated and we therefore consider Bayesian optimization appropriate, as it is known to give good optimization results on small data sets. Non-linear relationships between the synthesis parameters and the corresponding output of interest, the achieved overpotential, are expected. For this reason, a Gaussian process (GP) regression model with the squared exponential covariance function (aka. RBF kernel) [30] is chosen as the fit function. Given a good fit of the data, the GP model can provide mean (μ_{GP}) and uncertainty (σ_{GP}) predictions of the output for unobserved sets of synthesis parameters $\boldsymbol{x}$. These predictions can be used to identify new synthesis parameters that optimize the output by evaluating an acquisition function (f_{acq}) computed as μ_{GP} plus σ_{GP}, which is similar to the widely used GP-UCB algorithm [31]:

$$f_{\mathrm{acq}}(\boldsymbol{x}) = \mu_{GP}(\boldsymbol{x}) + \sigma_{GP}(\boldsymbol{x})$$

Where typical BO algorithms are often designed to automatically

identify a single set of input parameters with maximum potential, we instead applied a human-in-the-loop approach where a researcher uses a visualization of the f_{acq} to select a batch of new and interesting synthesis parameters (step 4 and 5 in Fig. 1). This enables the selection of multiple sets of inputs in every iteration that are both diverse and interesting. Consequently, this allows the researcher to perform multiple lab experiments in each iteration, which is also more practical. For simplicity a grid size of 1 was used.

2.2.1. Sensitivity analysis

Additionally, the fitted GP regression model can be utilized to identify the most important synthesis parameters by performing a global sensitivity analysis (SA). In this context, the input parameter sensitivity can be defined as the expected change of the output as a function of the input parameter [32]. We can compute this quantity empirically for each input parameter d with the GP as the mean squared derivative of the predicted output over a set of query points $\boldsymbol{x}_i$:

$$s_d^2(\boldsymbol{x}) = \frac{1}{N}\sum_{i=1}^{N}\left(\frac{\partial \mu_{GP}(\boldsymbol{x}_i)}{\partial x_{i,d}}\right)^2$$

The derivative in the above expression can be computed analytically or with automatic differentiation for a GP using the squared exponential covariance function. To enable direct comparison of input parameters with different scales, the inputs were normalized. In visual presentations of the sensitivities, we plotted the square root of the sensitivity s_d.

3. Results

3.1. Linear grid study

Before applying AI guided optimization a linear grid study was conducted, where all but one parameter was kept constant. This to investigate how temperature (T), current density (i) and deposition time (t) affect the deposited nanostructure and its electrochemical performance individually, and to establish a training data set for the optimization algorithm. For this study the parameter space was limited to cover 2–64 min, 5–160 mA cm^{-2} and 20–65 °C. A t of 5 min, i of 75 mA cm^{-2} and a T of 65 °C was used as standard parameters.

Fig. 2 (a–c) shows that the microstructure visually does not vary as function of t. On the other hand, the i and T changes the microstructure significantly as shown in Fig. 2 (d–f) and (g–i), respectively. At low current densities long spikes can be observed that become shorter and less pronounced when increasing the i. At low T the microstructure appears flat, a structure which coarsens with increasing T, until spikes start to form above 60 °C.

According to Fig. 2 only two out of three investigated synthesis parameters change the deposited microstructure. It was therefore expected to observe changes in the electrochemical performance for variations in i and T. As shown in Fig. 3, t and i changes the electrochemical performance significantly, while T, even though it changes the microstructure the most, does not affect the electrochemical performance much. For reference a bare perforated Ni plate on average requires an η_{10} of −321

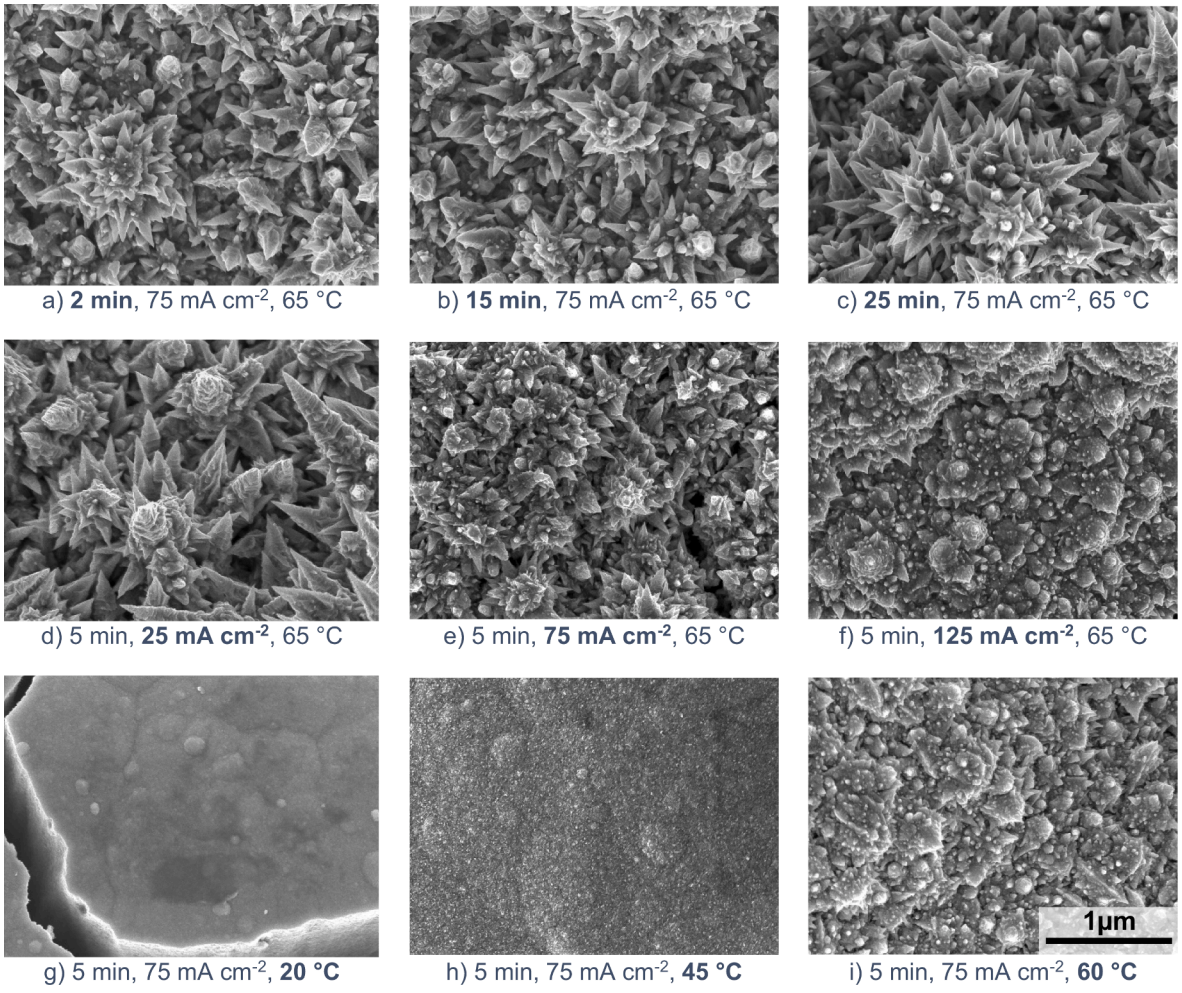

Fig. 2. SEM images illustrating how the synthesis parameters; **t** (a-c), **i** (d-f) and **T** (g-i) changes the deposited microstructure. From a-c the microstructure visually does not change suggesting that **t** only creates a thicker layer. From d-f the spike length decreases with increasing **i**, while the microstructure from g-i changes drastically from almost flat and sandpaper-like at low and intermediate **T** to spiky at high **T**.

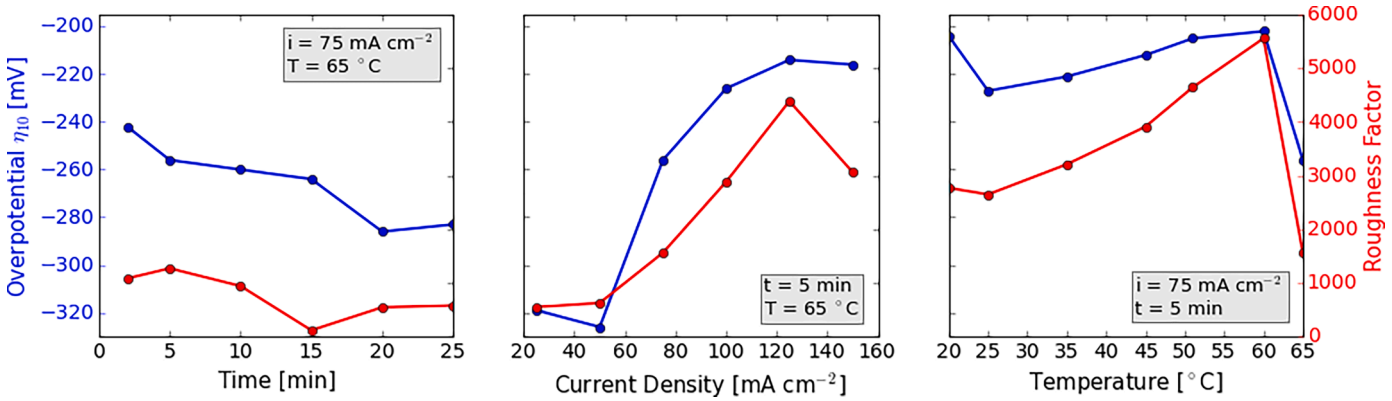

Fig. 3. η_{10} (blue) and R_f (red) as function of **t**, **i** and **T**. With the chosen parameters the **i** appears to be the most sensitive synthesis parameter, followed by time and **T**. η_{10} generally decreases with increasing R_f.

mV, showing that almost all structures deposited in this study improve the substrates performance.

Improvements in performance seen in Fig. 3 scale with the measured R_f, indicating that the variations arise due to a change in active surface area.

3.2. Optimization

To make good predictions concerning the synthesis parameters, the training data must be large and randomly spread across the search space. Initially, the linear grid study data served as training data, however, as shown in Fig. S2, it was based on a linear search grid and thus there are many underrepresented areas of the search space, inducing a high σ_{GP}. Additional samples were therefore made using randomised parameters, creating a dataset with 31 samples significantly lowering σ_{GP}. Subsequently, 3 iterations of the Bayesian Optimisation (BO) loop were performed. The test candidates were chosen from areas in the prediction model with comparatively low predicted η_{10}. It should be noted that testing parameter sets with high predicted η_{10} can be used to further validate the model in those areas. However, since the objective of this study is to optimize the achieved overpotentials with minimal experimental effort and the model already had relatively low uncertainty, this was deliberately omitted.

After fitting a GP regression model to the training data in step 4 of the BO loop (see Fig. 1) a sensitivity analysis was conducted, to investigate how the μ_{GP} of η_{10} changes as function of either T, i or t (see Fig. S3). Already the first iteration revealed that the mean η_{10} prediction only depends on two out of three investigated parameters: i and T. Since these two parameters were dominant, the optimisation problem reduced from a three- to two-dimensional problem. It was chosen to keep varying t randomly for the following iterations, however, since no time-sensitivity was found the t range was reduced after each iteration for practical reasons. This is a surprising finding and counter-intuitive, as one would expect the coating thickness to vary with t, and therefore also the availability of surface area obtained from porous coatings. For validation of this, sample 4 was synthesized again while reducing t from 30 min to 5 min, yielding practically identical results (see Fig. S4).

Fig. 4 shows heat maps of μ_{GP} and σ_{GP}, as well as f_{acq}. Two distinct areas with lower predicted η_{10} are found in all three iterations (brighter colours), centred approximately around (140 mA cm^{-2}, 55 °C) and (< 10 mA cm^{-2}, 25 °C). As the number of iterations and samples in the training data increases the model changes and σ_{GP} decreases. σ_{GP} for the first iteration is lowest around parameters frequently used in the linear grid study (75 mA cm^{-2} and 65 °C), and does not change significantly after iteration 2, indicating that a confident model has been established.

Throughout iteration 1 and 2 exploration and exploitation were conducted, while the area with the lowest η_{10} were exploited in the third iteration. The results (synthesis parameters, η_{10}, R_f) of all three iterations are summarized in Table 2.

As a general rule, samples synthesized with parameters in proximity to the μ_{GP} optima show the lowest η_{10}, indicating good agreement of experiment and prediction model.

Sample 4 showed the best performance in this study with $\eta_{10} = -129\ mV$. As expected, it also shows the highest R_f value (11,836), even though there is essentially no structuring visible in the SEM image in Fig. 5. This indicates that the porous, deposited layer exhibits features in the nanometre range, below the resolution limit of the microscope. Higher resolution microscopic techniques, e.g. STM, could be applied in future investigations to confirm that these nano-sized features are indeed present, but lie outside the scope of this study.

In Fig. 6 the LSV curves of the best sample (sample 4, green) are compared to LSV curves of perforated Ni plate substrate, Ni foam, Pt-foil and Raney Ni (on perforated Ni plate). Sample 4 outperforms all materials except Raney Ni. As higher current densities are reached, the sample approaches the Raney Ni domain.

Ni electroplating for HER catalysis has been exhaustively studied in the past. A comparison to several recent reports on such electrodes (Table 3) highlights the BO loops efficiency: a total of only 35 samples was sufficient to rival the best reported catalysts in this category, without prior knowledge of what a "good" set of parameters is for this specific synthesis route.

3.3. Four-dimensional parameter space optimization

Discovering the best sample after the first iteration in Section 3.2 can seem like a coincidence. To further explore the feasibility of the BO loop, a study using the method described in Section 2 was conducted with a modified setup and four parameters: in addition to i, t and T, the EDA concentration was varied in a range from 50 to 300 g L^{-1}. A sample with lower η_{10} than sample 4 (−117 mV @ 10 mA cm^{-2}) was found after 1 iteration and 30 additional samples (see Table S2), proving that ML can steer the scientists into the right direction fast and efficiently, whereafter only fine tuning of the synthesis parameters is needed. The prediction model, even though progressing differently, ultimately finds t to remain a non-sensitive parameter (no substantial dependency between η_{10} and t, Fig. 7). It also indicates that further improvement is possible e.g. by reducing the EDA concentration to approximately 220–230 g L^{-1} (Fig. 7). It should be noted that since there is no straight-forward visual representation of functions with four or more dimensions, the test candidates were chosen by visual comparison of the predicted η_{10} as a function of two parameters each. For true 4-parameter optimization, one could implement an optimization algorithm that outputs discrete 4-parameter sets with low predicted η_{10} values alongside the continuous prediction model.

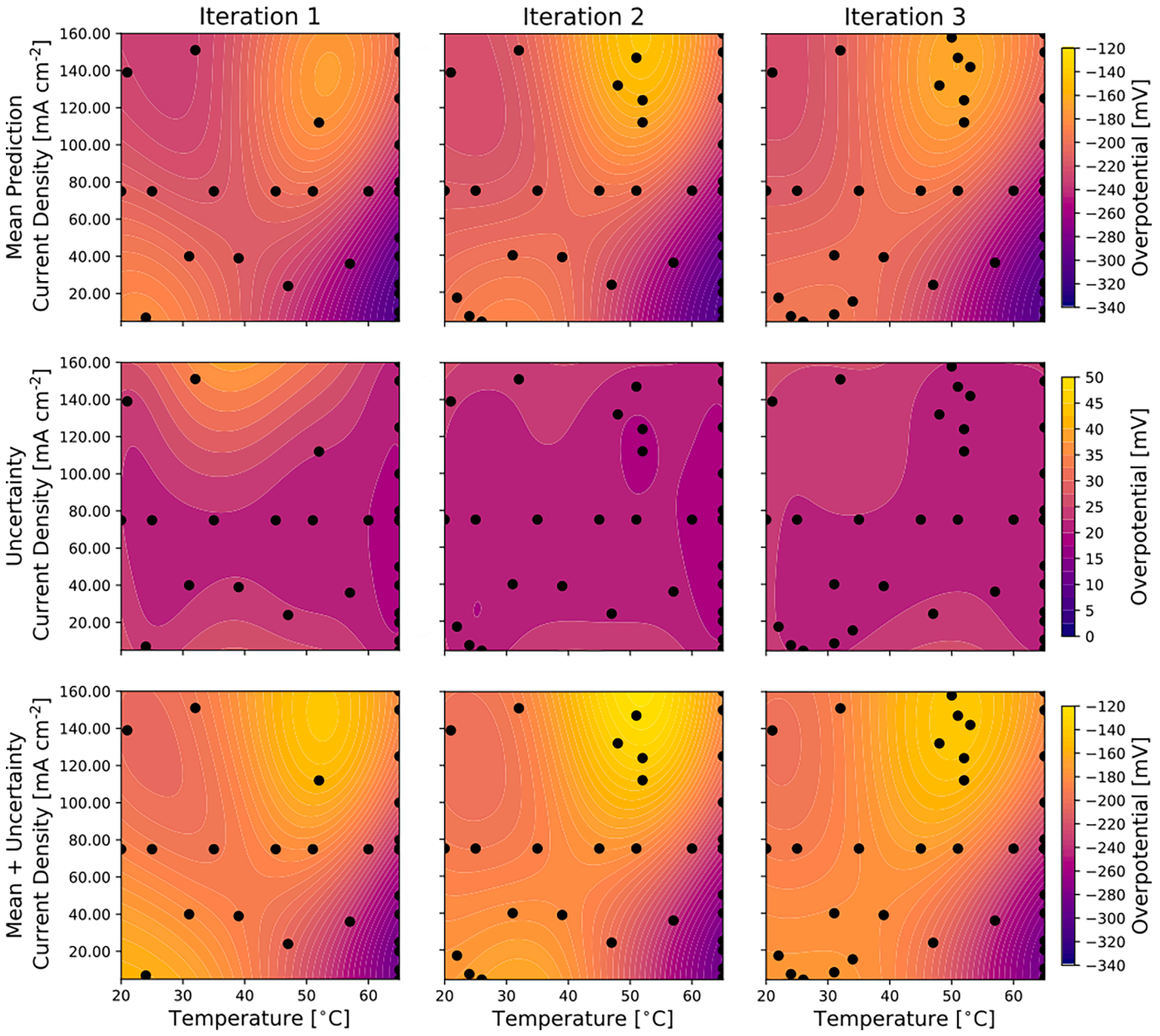

Fig. 4. Illustration of the established $\boldsymbol{\mu}_{GP}$, $\boldsymbol{\sigma}_{GP}$ and a plot of $\mathbf{f}_{acq}$, the ladder used to identify promising synthesis parameters. The model is based on known data points (31, 36 and 40 data points for iteration 1, 2 and 3 respectively) and shows the predicted $\boldsymbol{\eta}_{10}$ as function of $\mathbf{T}$ and $\mathbf{i}$. Brighter colors indicate a low $\boldsymbol{\eta}_{10}$and thus a good electrode performance. The figure shows that the prediction changes slightly and that the uncertainty is lowered with increasing number of iterations and samples.

4. Discussion

Over the course of this study, the application of ML for electrode development proved to be very effective: a substantial improvement of 204 mV over the performance of the Ni support was achieved iteratively in two separate instances, despite changes in the experimental setup.

In contrast to the linear grid study (Section 3.1), the sensitivity analysis of the ML optimization finds T to be the most influential parameter for the synthesis. This discrepancy could be explained by the fact that for the linear grid study, only one parameter was varied while the others were kept constant. Therefore, only the T dependency along a straight line in the three-dimensional phase space is taken into account. This could lead one to investigate under false assumptions, whereas the sensitivity analysis utilizes all measured results.

When reducing the synthesis time of the best performing samples from 30 min down to 5 min (Fig. S4), there is no significant reduction in performance nor any notable visual change of the sample surface. This indicates that the t mainly affects the layer thickness, while the microstructure stays the same. Also, it indicates that the porosity is homogeneous throughout the layer thickness and invariant to the synthesis time. Only the outermost part of the thicker layer is electrochemically active due to mass transport limitations. This effectively limits the maximum ECSA that can be achieved by this method and implies that even shorter deposition should be applicable while maintaining HER performance. Both the required time and material utilization are essential parameters for industrial production. Future studies should therefore also investigate the influence of deposition time on the structure and electrochemical performance as it approaches zero. This issue could potentially be bypassed by implementing a multi-step synthesis to achieve a pore size gradient throughout the layer to improve gas diffusion and allow deeper penetration of the layer.

Since there are no dopants added and XPS analysis revealed no residue from the precursors of the synthesis solution or contamination of iron from the temperature probe (see Fig. S6) that could affect HER

Table 2
Complete list of all the samples synthesized during the 3 iterations of the BO loop. In the table the measured η_{10} and R_f has been included as well.

Iter.	No.	Synthesis Parameters			η_{10} [mV]	R_f
		T [°C]	i [mA cm^{-2}]	t [min]		
1	1	22	17	23	−210	3684
	2	26	4	39	−194	4428
	3	48	132	16	−168	7635
	4	51	147	30	−129	11,836
	5	52	124	26	−144	5645
2	6	31	8	11	−220	3499
	7	34	15	24	−183	7903
	8	50	158	17	−180	6466
	9	53	142	8	−191	5249
	10	55	152	15	−180	5269
3	11	48	143	10	−166	7381
	12	49	126	4	−222	7513
	13	50	140	3	−241	3466
	14	51	146	7	−169	9358
	15	52	136	12	−178	6411
	16	52	170	6	−212	5061
	17	53	155	8	−211	4544

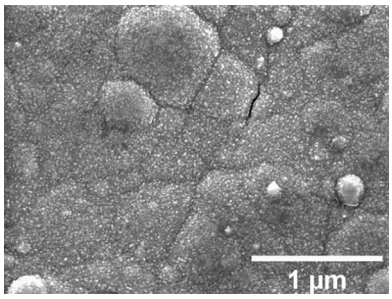

Fig. 5. SEM image of sample 4′s surface showing rough sandpaper-like features, which are hard to resolve further by SEM.

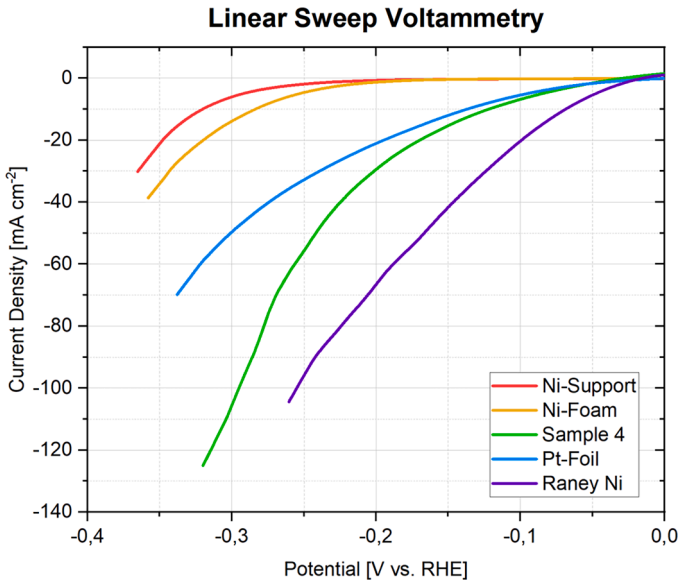

Fig. 6. Smoothened LSV curves for the substrate (red), Ni foam (yellow), Pt-foil (blue), best performing sample (sample 4, green) and Raney NiMo (NiMo, purple).

catalysis, it is reasonable to assume that the main factor for HER performance is the ECSA. This is confirmed by double-layer capacitance measurements (see Fig. S5) which show a logarithmic relationship between overpotential and surface roughness, as predicted by the Butler-Volmer equation. Ni perforated plates were chosen in this study because they are a commonly used substrate for technical electrodes, applied in commercial electrolyzers. Additionally, they offer relatively low cost, ease of handling and wide accessibility. Further reduction of the overpotential could be achieved with high surface area substrates such as Ni foams or meshes, which allow for higher absolute ECSA values.

Table 3
Short overview of different state of the art Ni electrodes. All electrodes have been synthesised using an electrodeposition method. The electrodes listed in the table have been tested in KOH at room temperature. Values marked with * have been determined manually from LSV curves.

Electrode Type	Substrate	KOH Conc [M]	η_{10} [mV]	Ref.
Ni Nano Particles	Ti	1	−197	[10]
Ni Nanocones	Cu	1	−215*	[5]
Ni Nanowire Array	Ti	1	−128	[11]
3D Ni Foams	Stainless Steel	8	−175*	[12]
Porous Ni	Ni	1	−243	[13]
Nanostructured Ni	Laser-treated Ni	1	−108	[14]
Sample 4	Perforated Ni	1	−129	This work

While higher T and i typically yield more porous structures, it is not intuitive how these synthesis variables, as well as the EDA crystal modifier, impact the Ni nucleation and growth mechanism. Other studies such as [33–36] have tried to investigate how and why synthesis parameters such as i, T, pH and bath composition affect the deposits morphology and properties, yet findings sometimes conflict. For instance, Ebrahimi et al. [34] state that a high i should promote grain refinement due to a resulting higher overpotential promoting nucleation. Besides, he found that Cziraki et al. [37] experienced the opposite in their studies. Therefore, it can be difficult to predict which combination of synthesis parameters yields low η_{10}, high porosity and ECSA. Implementing a AI based optimization process enabled us to find a performance maximum in considerably less iterations and with higher confidence as compared to a linear grid search. With the used grid spacing (1 mA cm^{-2}, 1 min, 1 °C, 50 g L^{-1}) a full linear grid search in the defined range would comprise over 2 million parameter sets. It is clear that in a real manual study the researcher would rule out many combinations for impracticality or from scientific intuition and the actual number of experiments would be much smaller – however it is also evident that such a linear grid search would still be impossible. This work shows that computational guidance can enable us to explore far more complex search spaces than traditionally feasible, by pointing to their most promising regions and thus avoiding unnecessary experimental effort. This effect will be exacerbated as the number of parameters is increased, e.g. in the case of multi-metal coatings.

5. Conclusion

In this work it has been shown that an EDA modulated Ni electrodeposition method can be used to synthesize nano porous, high-performance HER electrodes. The method allows for precise control over the layer thickness and morphology, ranging from micrometre-sized, star-shaped features to sandpaper-like structures with specific surface areas and overpotentials (−129 and −117 mV @ 10 mA cm^{-2}) approaching the best known technical high surface area electrodes such as Raney Ni. Implementation of a ML assisted optimization process enabled us to find a performance-maximum twice in considerably less experimental iterations than what would have been necessary with a linear grid search, due to the unintuitive interdependencies of the synthesis variables.

Funding

The financial support from the Independent Research Fund of Denmark through the “Hydrogen in demand – (H2Now)” project (grant

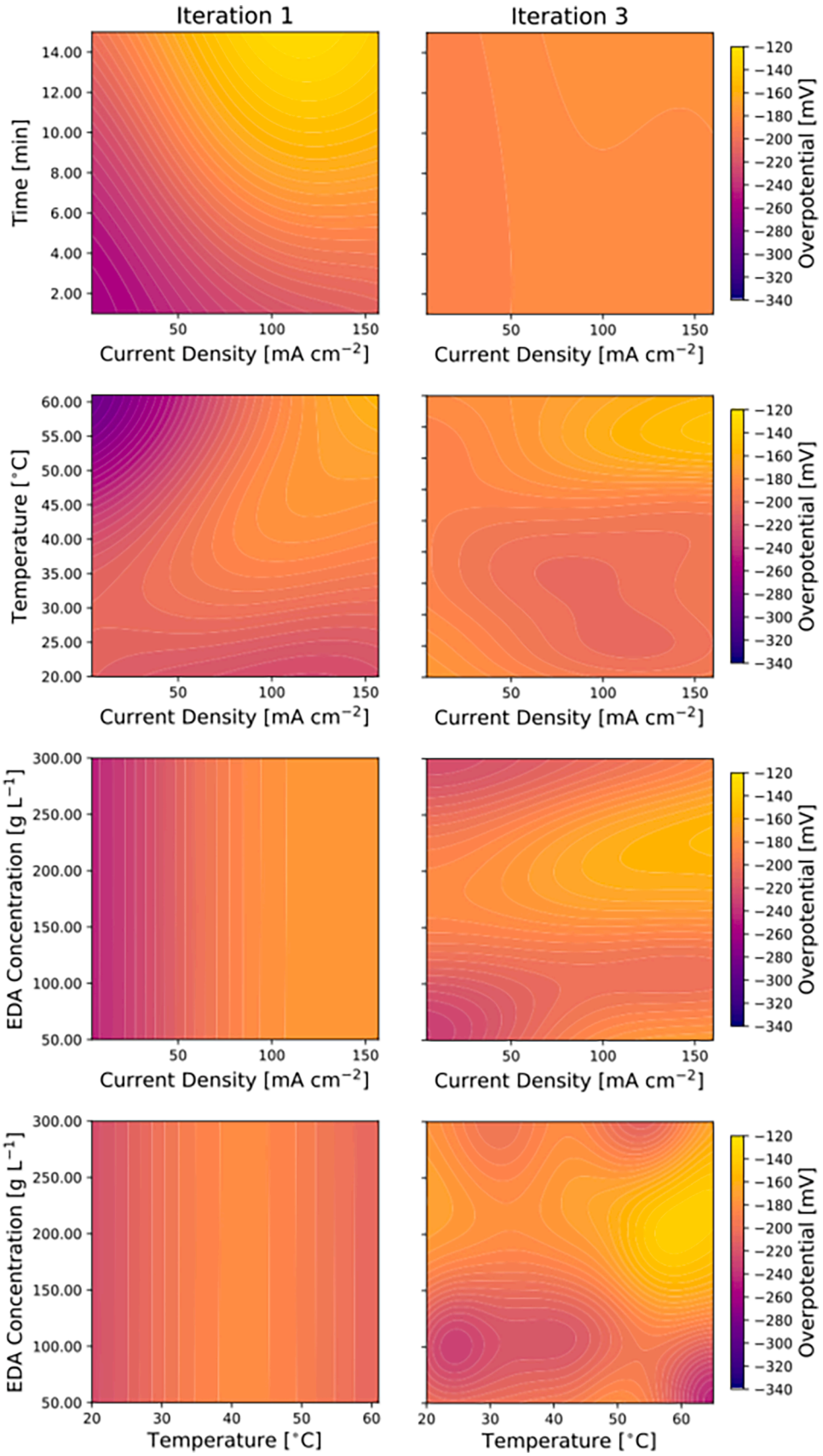

Fig. 7. Illustration of f_acquisition used to identify promising synthesis parameters. The model is based on known data points from Table S2 and shows the predicted η_{10} as function of four parameters, T, i, t and EDA concentration. Brighter colors indicate a low $\boldsymbol{\eta}_{10}$and thus a good electrode performance.

number 9041–00334B) and the DTU Alliance project "SeaCat" are gratefully acknowledged.

Data availability

The raw data required to reproduce these findings are available to download from https://sciencedata.dk/shared/dtu.dk/1bd88f16a9c8efb0d4d3a583bc75cc26. The processed data required to reproduce these findings cannot be shared at this time due to time limitations.

Author statement

V.H.J. carried out experiments and data analysis except for the 4-parameter study and XPS measurements. S.M.S., E.J. and E.H.C. carried out the experiments for the 4-parameter study. E.M. carried out XPS measurements. R.K., M.K. and E.M. supervised the experimental work. A.B. supervised and J.B. carried out the machine learning optimization. V.H.J. and E.M. wrote the original manuscript draft, with J.B. and A.B. contributing the ML related sections. All authors discussed the results and contributed to the final manuscript.

Declaration of Competing Interest

The authors declare that they have no known competing financial interests or personal relationships that could have appeared to influence the work reported in this paper.

Supplementary materials

Supplementary material associated with this article can be found, in the online version, at doi:10.1016/j.apmt.2023.102005.

References

[1] T. Skoczkowski, E. Verdolini, S. Bielecki, M. Kochański, K. Korczak, A. Węglarz, Technology innovation system analysis of decarbonisation options in the EU steel industry, Energy 212 (2020), https://doi.org/10.1016/j.energy.2020.118688.
[2] A. Nurdiawati, F. Urban, Towards deep decarbonisation of energy-intensive industries: a review of current status, technologies and policies, Energies 14 (9) (2021), https://doi.org/10.3390/en14092408 (Basel).
[3] IEA (2021), *Global Hydrogen Review 2021*, IEA, Paris https://www.iea.org/reports/global-hydrogen-review-2021, License: CC BY 4.0.
[4] Y. Guo, G. Li, J. Zhou, Y. Liu, Comparison between hydrogen production by alkaline water electrolysis and hydrogen production by PEM electrolysis, IOP Conf. Ser. Earth Environ. Sci. 371 (4) (2019), 042022, https://doi.org/10.1088/1755-1315/371/4/042022.
[5] G.B. Darband, M. Aliofkhazraei, A. Sabour Rouhaghdam, Nickel nanocones as efficient and stable catalyst for electrochemical hydrogen evolution reaction, Int. J. Hydrog. Energy 42 (21) (2017) 14560–14565, https://doi.org/10.1016/j.ijhydene.2017.04.120.
[6] P. Frink, Hydrogen energy storage study, IDC Clean Energy Proj. Prep. Advis. Serv. (2018).
[7] C. González-Buch, I. Herraiz-Cardona, E. Ortega, J. García-Antón, V. Pérez-Herranz, Synthesis and characterization of macroporous Ni, Co and Ni–Co electrocatalytic deposits for hydrogen evolution reaction in alkaline media, Int. J. Hydrog. Energy 38 (25) (2013) 10157–10169, https://doi.org/10.1016/j.ijhydene.2013.06.016.
[8] A.K. Cheong, A. Lasia, J. Lessard, Study of the mechanism of the hydrogen evolution reaction at raney nickel electrodes in the presence of organic compounds, J. Electrochem. Soc. 141 (4) (1994) 975–982, https://doi.org/10.1149/1.2054867.
[9] E. Hatami, A. Toghraei, G. Barati Darband, Electrodeposition of Ni–Fe micro/nano urchin-like structure as an efficient electrocatalyst for overall water splitting, Int. J. Hydrog. Energy 46 (14) (2021) 9394–9405, https://doi.org/10.1016/j.ijhydene.2020.12.110.
[10] S. Tao, F. Yang, J. Schuch, W. Jaegermann, B. Kaiser, Electrodeposition of nickel nanoparticles for the alkaline hydrogen evolution reaction: correlating electrocatalytic behavior and chemical composition, ChemSusChem 11 (5) (2018) 948–958, https://doi.org/10.1002/cssc.201702138.
[11] X. Feng, et al., Nickel nanowire arrays with preferential orientation for boosting hydrogen evolution reaction capability, J. Electrochem. Soc. 167 (10) (2020), 106501, https://doi.org/10.1149/1945-7111/ab9756.
[12] K.I. Siwek, S. Eugénio, D.M.F. Santos, M.T. Silva, M.F. Montemor, 3D nickel foams with controlled morphologies for hydrogen evolution reaction in highly alkaline media, Int. J. Hydrog. Energy 44 (3) (2019) 1701–1709, https://doi.org/10.1016/j.ijhydene.2018.11.070.
[13] C. Xu, et al., Porous nickel electrodes with controlled texture for the hydrogen evolution reaction and sodium borohydride electrooxidation, CrystEngComm 22 (25) (2020) 4228–4237, https://doi.org/10.1039/D0CE00344A.
[14] I.A. Poimenidis, et al., Electrodeposited laser – nanostructured electrodes for increased hydrogen production, Int. J. Hydrog. Energy 47 (16) (2022) 9527–9536, https://doi.org/10.1016/j.ijhydene.2022.01.062.
[15] T.W. David, H. Anizelli, T.J. Jacobsson, C. Gray, W. Teahan, J. Kettle, Enhancing the stability of organic photovoltaics through machine learning, Nano Energy 78 (2020), 105342, https://doi.org/10.1016/j.nanoen.2020.105342.
[16] C. Chen, Y. Zuo, W. Ye, X. Li, Z. Deng, S.P. Ong, A critical review of machine learning of energy materials, Adv. Energy Mater. 10 (8) (2020), 1903242, https://doi.org/10.1002/aenm.201903242.
[17] A. Bhowmik, et al., Implications of the BATTERY 2030+ AI-Assisted toolkit on future low-TRL battery discoveries and chemistries, Adv. Energy Mater. 12 (17) (2022), 2102698, https://doi.org/10.1002/aenm.202102698.
[18] Z. Wang, H. Zhang, J. Li, Accelerated discovery of stable spinels in energy systems via machine learning, Nano Energy 81 (2021), 105665, https://doi.org/10.1016/j.nanoen.2020.105665.
[19] M. Vogler, et al., Brokering between tenants for an international materials acceleration platform, ChemRxiv (2022).
[20] Z. Yao, et al., Machine learning for a sustainable energy future, Nat. Rev. Mater. 8 (3) (2022) 202–215, https://doi.org/10.1038/s41578-022-00490-5.
[21] C.J. Taylor, et al., A brief introduction to chemical reaction optimization, Chem. Rev. 123 (6) (2023) 3089–3126, https://doi.org/10.1021/acs.chemrev.2c00798.
[22] B.J. Shields, et al., Bayesian reaction optimization as a tool for chemical synthesis, Nature 590 (7844) (2021) 89–96, https://doi.org/10.1038/s41586-021-03213-y.
[23] N.H. Angello, et al., Closed-loop optimization of general reaction conditions for heteroaryl Suzuki-Miyaura coupling, Science 378 (6618) (2022) 399–405, https://doi.org/10.1126/science.adc8743 (1979).
[24] Z. Liu, et al., Machine learning with knowledge constraints for process optimization of open-air perovskite solar cell manufacturing, Joule 6 (4) (2022) 834–849, https://doi.org/10.1016/j.joule.2022.03.003.
[25] D. Bash, et al., Multi-fidelity high-throughput optimization of electrical conductivity in P3HT-CNT composites, Adv. Funct. Mater. 31 (36) (2021), 2102606, https://doi.org/10.1002/adfm.202102606.
[26] Y. Zhao, et al., Machine learning assisted design of experiments for solid state electrolyte lithium aluminum titanium phosphate, Front. Mater. 9 (2022), https://doi.org/10.3389/fmats.2022.821817.
[27] C.H. Liow, et al., Machine learning assisted synthesis of lithium-ion batteries cathode materials, Nano Energy 98 (2022), 107214, https://doi.org/10.1016/j.nanoen.2022.107214.
[28] W. Zhou, Z. Zheng, C. Wang, Z. Wang, R. An, One-step fabrication of 3D nanohierarchical nickel nanomace array to sinter with silver NPs and the interfacial analysis, ACS Appl. Mater. Interfaces 9 (5) (2017) 4798–4807, https://doi.org/10.1021/acsami.6b13031.
[29] P. Connor, J. Schuch, B. Kaiser, W. Jaegermann, The determination of electrochemical active surface area and specific capacity revisited for the system MnOx as an oxygen evolution catalyst, Z. Phys. Chem. 234 (5) (2020) 979–994, https://doi.org/10.1515/zpch-2019-1514.
[30] C.E. Rasmussen, K.I. Williams, Gaussian Processes For Machine learning, ISBN 026218253X, MIT Press, 2006.
[31] N. Srinivas, A. Krause, SM. Kakade, M. Seeger, Gaussian process optimization in the bandit setting: no regret and experimental design, in: Proceedings of the 27th International Conference on Machine Learning, 2010, pp. 1015–1022.
[32] W.A. Appiah, J. Busk, T. Vegge, A. Bhowmik, Sensitivity analysis methodology for battery degradation models, Electrochim. Acta 439 (2023), 141430, https://doi.org/10.1016/j.electacta.2022.141430.
[33] A. Boukhouiete, S. Boumendjel, N.E.H. Sobhi, Effect of current density on the microstructure and morphology of the electrodeposited nickel coatings, TUrk. J. Chem. 45 (5) (2021) 1599–1608, https://doi.org/10.3906/kim-2102-46.
[34] F. Ebrahimi, Z. Ahmed, The effect of current density on properties of electrodeposited nanocrystalline nickel, J. Appl. Electrochem. 33 (8) (2003) 733–739, https://doi.org/10.1023/A:1025049802635.
[35] J.M. Lee, K.K. Jung, J.S. Ko, Effect of NaCl in a nickel electrodeposition on the formation of nickel nanostructure, J. Mater. Sci. 51 (6) (Mar. 2016) 3036–3044, https://doi.org/10.1007/s10853-015-9614-8.
[36] X. Yu, J. Yang, X. Ren, Z. Sui, Influences of pH and EDTA additive on the structure of Ni films electrodeposited by using bubble templates as electrocatalysts for hydrogen evolution reaction, Membranes 11 (3) (2021) 165, https://doi.org/10.3390/membranes11030165.
[37] Á. Cziráki, B. Fogarassy, I. Geröcs, E. Tóth-Kádár, I. Bakonyi, Microstructure and growth of electrodeposited nanocrystalline nickel foils, J. Mater. Sci. 29 (18) (1994) 4771–4777, https://doi.org/10.1007/BF00356522.

Veronica Humlebæk Jensen holds a M.Sc.Eng. (2022) in Physics and Nanotechnology from the Technical University of Denmark. In January 2023 she joined the Department of Energy Conversion and Storage at the Technical University of Denmark as a PhD student. Her research focuses on development of oxygen evolution reaction electrodes, which can lower the operating temperature in solid oxide electrolysis cells.

Enzo Moretti obtained his Master's degree in physics from the University of Heidelberg in 2017. During his Master's studies and subsequent work in industrial battery development he focused on the synthesis of hierarchically structured Li-ion battery cathodes and solid electrolytes. Since 10/2020 he is a Ph.D. student at the Department of Energy Conversion and Storage of the Technical University of Denmark. His-research focus is on the design and synthesis of catalysts and electrodes for alkaline sea water electrolysis. Additionally, his work is concerned with autonomous experimentation for accelerated materials discovery.

Jonas Busk obtained a master's degree in software development from IT-University of Copenhagen (ITU) in 2015. He received a Ph.D. degree in machine learning from Technical University of Denmark (DTU), Department of Applied Mathematics and Computer Science (DTU Compute), in 2019. In 2020, he joined the Department of Energy Conversion and Storage (DTU Energy), where he is currently working as a postdoctoral researcher. His-research focus on the development and application of advanced machine learning methods in the field of materials discovery for energy conversion and storage, including Bayesian optimisation methods and structural optimisation and simulation of materials using equivariant neural network models.

Emil Howaldt obtained his bachelor degree at DTU Electro in Sustainable Energy Design in 2020. He is currently studying a Master's degree in Energy conversion and storage which will be finished 02/2023. His-main research focus is on Power-2-X technologies, with the main focus on the synthesis of catalysts to be used in both electrolysis and fuel cells.

Sofie Marie Skov obtained her Bachelor's degree from the Technical University of Denmark in 2021/06. From 2021/09-today, she studies at the Technical University of Denmark and finalizes her master's degree in Sustainable Energy with focus on energy conversion and storage.

Emilie Jacobsen obtained her Bachelor's degree from the Technical University of Denmark in 2021/06. From 2021/09-today, she studies at the Technical University of Denmark and finalizes her master's degree in Sustainable Energy with focus on energy conversion and storage.

Mikkel Kraglund studied Physics at the Technical University of Denmark (DTU), and obtained his Bachelor's degree in 2011 and Master's degree in 2014. In 2017 he obtained his Ph.D. degree from the Department of Energy Conversion and Storage at DTU, with a project on alkaline electrolysis. The Ph.D. program included a research stay at Forschungszentrum Jülich. Since obtaining his Ph.D. degree he has continued to work on alkaline electrolysis, with a focus on electrode and catalyst development, membrane development, and cell testing and characterization. He is now working as a research engineer.

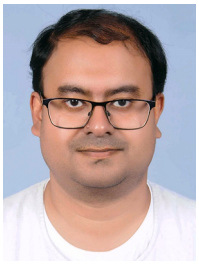

Arghya Bhowmik is a tenure-track professor of autonomous materials discovery at the Department of Energy Conversion and Storage, Technical University of Denmark. His-research focuses on automating materials development with generative deep learning and physics based simulations. His-group builds and applies methods for data driven models for scale bridged simulations of energy materials. He is co-PI in several large scale collaborative research projects focused on machine learning-based multi time/length scale inverse design like leading the "Battery Interface Genome" of the EU-H2020 BIG-MAP project and 'atom to system' differentiable digital twin effort in Capex pioneer centre, Denmark.

Ragnar Kiebach is a Professor at the Technical University of Denmark, where he leads a section on ceramic processing. He obtained his Ph.D. d from the Christians-Albrechts University in Kiel, Germany. Following that, he conducted postdoctoral research at the Instituto Nacional de Astrofísica, Óptica y Electrónica in Puebla, Mexico. In 2009, he continued his career as a postdoc and Senior Researcher at the National Laboratory for Sustainable Energy, Denmark. His-primary research interest lies in sustainable production of nanostructured materials for energy conversion and ceramic processing. Currently, he focuses on advanced functional materials processing, and prototyping for electrolysis and fuel cells.